SolarPACES 2022, 28th International Conference on Concentrating Solar Power and Chemical Energy Systems
Receivers and Heat Transfer Media and Transport: Point Focus Systems
https://doi.org/10.52825/solarpaces.v1i.693

Published: 20 Dec. 2023

Control Concept for a Molten Salt Receiver in Star Design

Development, Optimization and Testing with Cloud Passage Scenarios

Jonas Schulte[1][https://orcid.org/0000-0001-9923-1703], Christian Schwager[1][https://orcid.org/0000-0002-4515-886X], Cathy Frantz[2][https://orcid.org/0000-0002-3455-3311], Felix Schloms[2][https://orcid.org/0000-0002-9443-5261], Cristiano J. Teixeira Boura[1][https://orcid.org/0000-0003-1854-1019], and Ulf Herrmann[1][https://orcid.org/0000-0002-6938-0860]

[1] Solar-Institut Jülich of the FH Aachen University of Applied Sciences, Germany

[2] Institute of Solar Research, German Aerospace Center, Germany

Abstract. A promising approach to reduce the system costs of molten salt solar receivers is to enable the irradiation of the absorber tubes on both sides. The star design is an innovative receiver design, pursuing this approach. The unconventional design leads to new challenges in controlling the system. This paper presents a control concept for a molten salt receiver system in star design. The control parameters are optimized in a defined test cycle by minimizing a cost function. The control concept is tested in realistic cloud passage scenarios based on real weather data. During these tests, the control system showed no sign of unstable behavior, but to perform sufficiently in every scenario further research and development like integrating Model Predictive Controls (MPCs) need to be done. The presented concept is a starting point to do so.

Keywords: Molten Salt Receiver, Star Design, Control Optimization, Cloud Passages

1. Introduction

Molten salt towers remain the leading technology in central receiver power plants today. Despite the advanced state of the technology, there is still high cost reduction potential. The star design pursues the approach of enabling the irradiation of the absorber tubes on both sides. That leads to a higher aperture surface area per used mass unit of high temperature alloys and thus to lower receiver system costs [1]. However, the star-shaped arrangement of the panels and their special interconnection lead to new requirements regarding the control system of the receiver. The salt flow from the inlet tank is divided into two flow paths. The mass flow through each of the flow paths is manipulated by a control valve. The salt streams merge again after they have passed the first two wings of the receiver. Then the salt flows through the third wing and enters the outlet tank. In common external molten salt receivers, the salt flow is also divided into two flow paths, but they just merge again at the very end of the receiver, so that the flow paths are hydraulically decoupled. In the case of the presented star receiver, the flow paths are hydraulically coupled. For example in cases in which the mass flow in wing 1 is reduced by closing the control valve in that flow path, the control valve in the other flow path also needs to close a bit to keep the mass flow constant. The hydraulic coupling leads to direct feedback between the individual control loops and thus to an increased risk of instability and oscillations. Figure 1 shows the configuration of the investigated system.

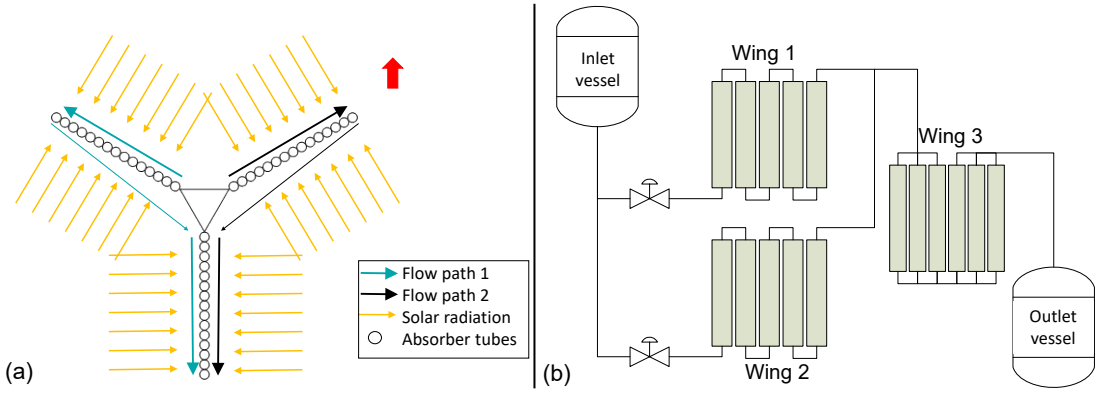

Figure 1. (a) Schematic sketch of a receiver in star design, (b) simplified Process Flow Diagram (PFD) of the receiver system.

This paper presents a control concept for a utility-scale molten salt tower receiver in a star design. The primary focus is on developing a stable and functional control system as simple as possible. The central tasks of the control system are to control the outlet temperature of the receiver and to minimize the temperature difference between the two parallel flow paths at the first two wings of the receiver in every operating condition. In this paper, the main quality criterion is the ability of the control system to keep the outlet temperature as close to the setpoint as possible during volatile radiation conditions.

2. Control System

The control system consists of four controllers. Figure 2 shows the layout of the control system. Two mass flow controllers, which manipulate the opening of the control valves, a temperature controller that defines the overall mass flow through the receiver, and a temperature difference controller that minimizes the temperature difference at the point at which the two parallel flow paths mix together by adjusting the mass flow difference between the two flow paths. All used feedback controllers are limited PID controllers.

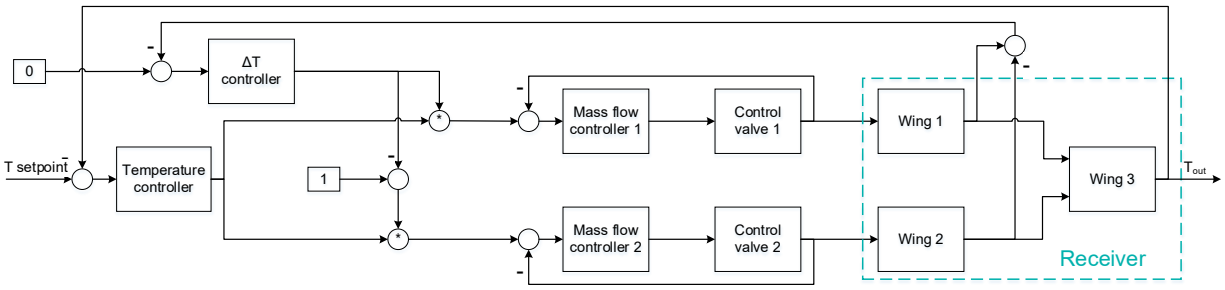

Figure 2. Schematic drawing of the control system.

Simple feedback and feedforward controllers struggle with controlling the outlet temperature in volatile radiation conditions because the molten salt usually needs between one and ten minutes to pass through the receiver [2], [3]. Although radiating the absorber tubes from both sides has the potential to lower the delay time, because the applied mass flow per absorber tube is higher, the delay remains the main challenge for the control system. To reduce the deviation of the outlet Temperature from the setpoint during fast changes in the flux density, as they appear as the result of cloud passages, a feedforward controller is included in the temperature and the temperature difference controller. The feedforward controllers calculate the overall mass flow and the mass flow distribution based on steady-state energy balances. For that purpose, it is assumed that the receiver system is equipped with real time flux density monitoring.

3. Control optimization

To evaluate the controller quality as objectively as possible, a cost function is defined for a test cycle of radiation steps on the receiver system. Conventional cost functions that are widely used in control systems like the Integral Squared Error (ISE) are symmetric and do not take into consideration that in molten salt systems, exceeding the setpoint has higher technical costs then falling below it. This is caused by the decomposition reaction of the commonly used nitrate salt mixture “solar salt” at higher temperatures and its effects on metal corrosion [4]. That is why an asymmetric cost function was defined. Apart from asymmetry, the function should also be progressive over the absolute value of the error. For control errors smaller than zero (the actual value is lower than the setpoint), the time derivative of the cost function is given by the following equation:

$$\frac{\mathrm{d}C}{\mathrm{d}t} = \ln\left(\left(\frac{\Delta y}{4}\right)^2 + 1\right) \cdot 2 \tag{1}$$

With C as the costs and Δy as the actual control error. For control errors greater than zero (the actual value is higher than the setpoint), the time derivative of the cost function is defined as follows:

$$\frac{\mathrm{d}C}{\mathrm{d}t} = \ln\left(\left(\frac{\Delta y}{3}\right)^2 + 1\right) \cdot 5 \tag{2}$$

Figure 3 shows the curve of the time derivative of the cost function depending on the control error.

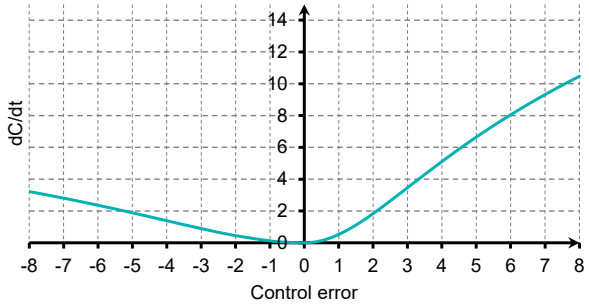

Figure 3. Time derivative of the cost function.

The given function is not to be understood as the only possible cost function for this optimization problem. Every function that is asymmetric, progressive over the absolute value of the error, and can be stably implement into the dynamic model is suitable.

For tuning the preliminary control parameters and testing the control stability, a simple dynamic model of the receiver is implemented with the object-oriented modeling language Modelica in the environment Dymola. The simplified model only represents the energy balance, the delay due to salt transport, and the dynamic behavior of the control valves. Inlet and outlet tank are represented by pressure boundaries, assuming that the pressure and level control in the tanks work ideally. As a first approach, the control parameters are tuned manually. To optimize and test the control parameters under realistic conditions a detailed dynamic model of the receiver is developed. This advanced dynamic model is based on previous research by Schwager et al. [5]. Every wing of the receiver is discretized in two dimensions. The model takes dynamic energy losses, the solar flux distribution, and infrared radiation exchange between the wings into consideration. The control system with its preliminarily tuned parameters is transferred to the detailed model. Because the detailed model also considers energy

losses, the feedforward control cannot be transferred from the simplified model to the detailed model without modification. For the correct calculation of the needed mass flow, a term for the receiver efficiency needs to be added. The following equation gives the feedforward signal:

$$\dot{m}_{\mathrm{ff}}=\eta_{\mathrm{th}}\frac{\dot{Q}_{\mathrm{abs}}}{c_{\mathrm{p}}\Delta T} \tag{3}$$

With η_{th} as the thermal efficiency of the receiver, $\dot{Q}_{\mathrm{abs}}$ as actual absorbed solar power, and ΔT as the temperature difference between the inlet and outlet of the receiver. The thermal efficiency is determined as follows:

$$\eta_{\mathrm{th}}=\frac{\dot{m}c_{\mathrm{p}}\Delta T}{\dot{Q}_{\mathrm{abs}}}=\frac{\dot{Q}_{\mathrm{abs}}-\dot{Q}_{\mathrm{loss}}}{\dot{Q}_{\mathrm{abs}}} \tag{4}$$

This results in the following equation for the feedforward signal.

$$\dot{m}_{\mathrm{ff}}=\frac{\dot{Q}_{\mathrm{abs}}-\dot{Q}_{\mathrm{loss}}}{c_{\mathrm{p}}\Delta T} \tag{5}$$

Figure 4 shows the determined energy loss characteristics of the star receiver and the linear fit function that is used in the feedforward controller.

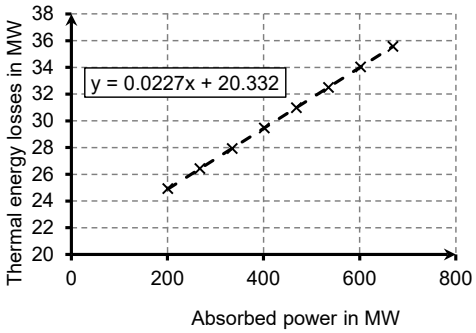

Figure 4. Energy loss characteristics of the star-receiver.

The final optimization of the control parameters is done by minimizing the costs for a defined test scenario of radiation steps in dependency of all nine control parameters with the Nelder-Mead-method. The Nelder-Mead method is a downhill simplex approach that does not need to determine derivatives [6]. Figure 5 shows the flux trends of the optimization scenario.

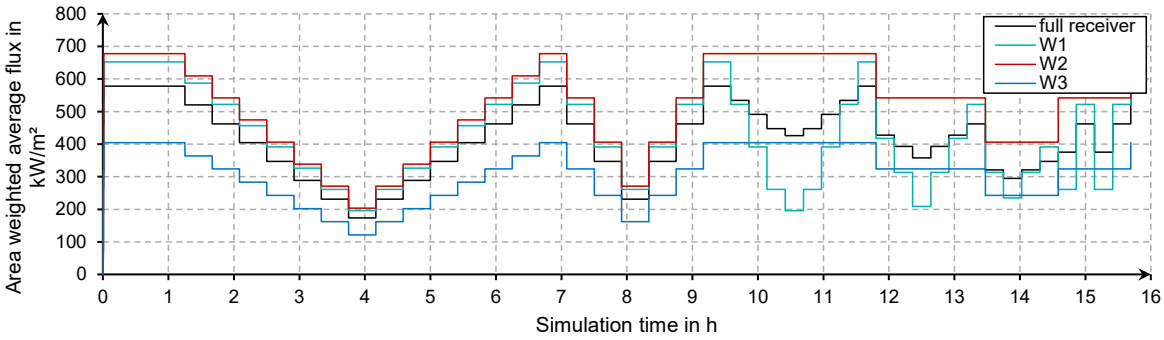

Figure 5. Generic test scenario of flux steps on the receiver for the control optimization.

The scenario is generic and was developed to have flux steps up and down of different heights, covering a wide range of load cases. The flux distribution between the first two wings of the receiver is also varied. Table 1 shows the control parameters before optimization like they were tuned manually in the simplified test system and after the optimization.

Table 1. Control parameters before and after optimization.

Variable	Before optimization	After optimization
Both mass flow controllers		
k	0.0061	0.0086288
T_i	10	2.4717
T_d	1.8	0.2050
Temperature controller		
k	5	14.8098
T_i	100	160.9481
T_d	0.001	0.001337
Temperature difference controller		
k	-0.0005	-0.0006834
T_i	8000	5810.0215
T_d	0.005	0.004504

4. Radiation data and cloud modeling

Real weather data is used to create a realistic test scenario for the control system. Based on DNI maps of an 8x8 km² area, with a spatial resolution of 20x20 m² and a time resolution of 30 s, the shading of the heliostat field is calculated for each time step. The DNI-maps are sourced from an all sky imager based nowcasting system by Nouri et al. [7]. To determine the resulting flux density on the receiver, the heliostat field is divided into six parts. Each part is assigned to one side of a wing. The nominal flux density distribution on the receiver, which was determined by raytracing simulations in the environment STRAL, is scaled depending on the area-weighted average of the Clear Sky Index (CSI) in the area of each heliostat cluster. Figure 6 shows the parts and the assignment of the heliostat field as well as an exemplary DNI map with clouds.

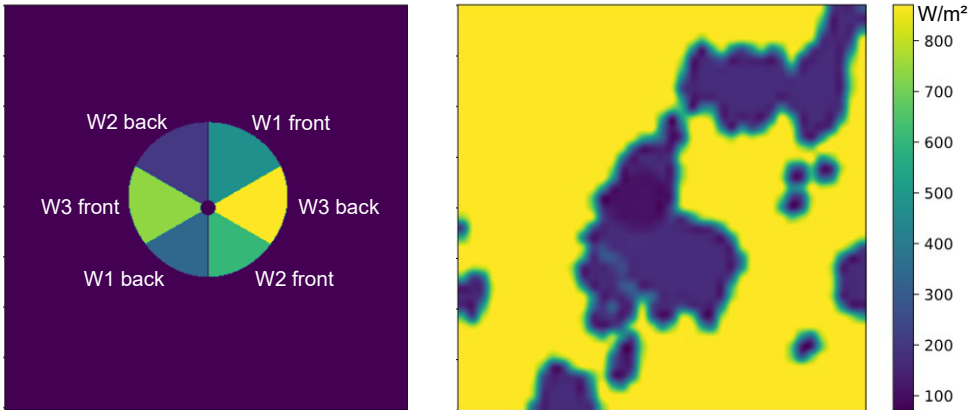

Figure 6. (a) Clustering of the heliostat field, (b) exemplary matching DNI-map, both maps 8x8 km² with a spatial resolution of 20x20m².

The assignment assumed in Figure 6 does not necessarily comply with the actual heliostat assignments to aim points at the receiver. The method presented in this work is just meant to produce realistic radiation time trends for testing the control system, without the necessity of computational expensive ray tracing simulations. It does not model the causal relationship between the used weather data and the applied flux on the receiver accurately. The calculation of the heliostat field shading leads to the flux trends shown in Figure 7.

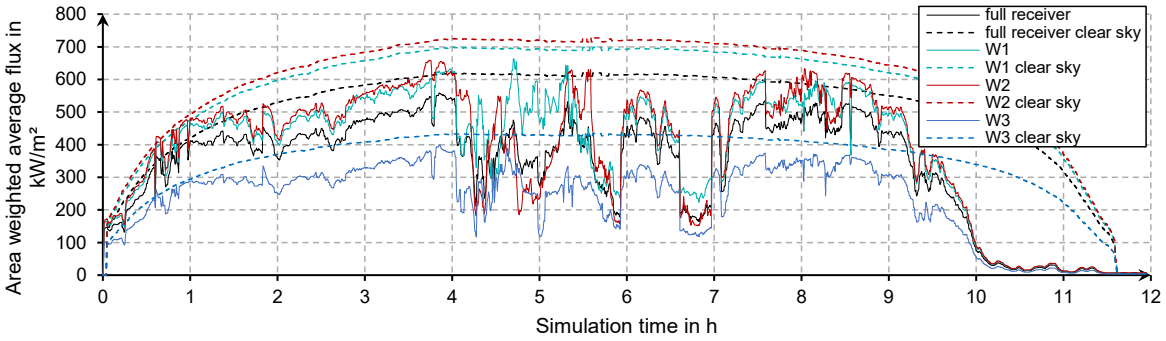

Figure 7. Resulting flux trends for the test scenario.

Figure 7 shows the area weighted-average of the flux on each wing of the receiver. For proper contextualization Figure 7 also shows which flux time series the used method provides for clear sky conditions.

5. Test results

Figure 8 shows the outlet temperature trends of the receiver wings and the temperature difference trend for the optimized control system tested with the previously described cloud scenario.

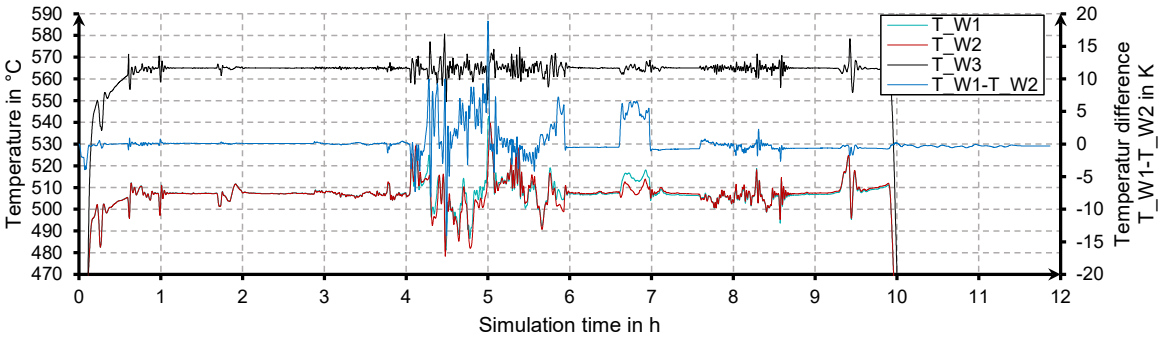

Figure 8. Outlet temperature trends of the receiver wings and temperature difference between the first two wings during the cloud passage test cycle.

There are only moderate radiation gradients during the first hours. During this time, there is almost no deviation from the setpoint. In the time period from the fourth to the sixth hour, there are several sharp radiation steps causing periods with high positive and negative temperature control errors. Those are occurring especially when there is a mass flow difference between the first two wings of the receiver (see Figure 9) caused by high flux differences (see Figure 7).

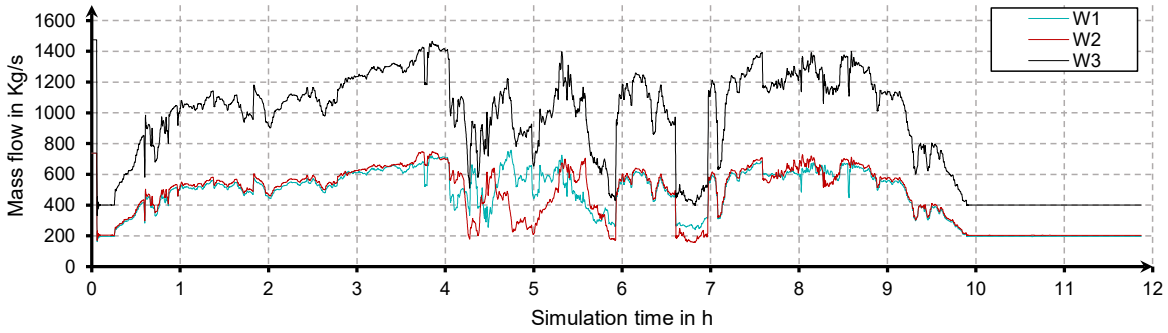

Figure 9. Mass flow trends of the receiver wings during the cloud passage test cycle.

To illustrate these results, Figure 10 shows the magnitudes of the occurring control errors and the corresponding accumulated time in which they occurred, for the control system before and after the parameter optimization. The measurement started when one of the systems reached the setpoint for the first time and was ended just when the temperature dropped due to the low solar radiation. All errors whose magnitude is lower than 4 K are neglected because they are assumed to be acceptable. With the optimized parameter set, the accumulated time in which control errors with a magnitude greater than 4 K occur is lower. The maximum of the positive control errors is also lower for the optimized parameter set.

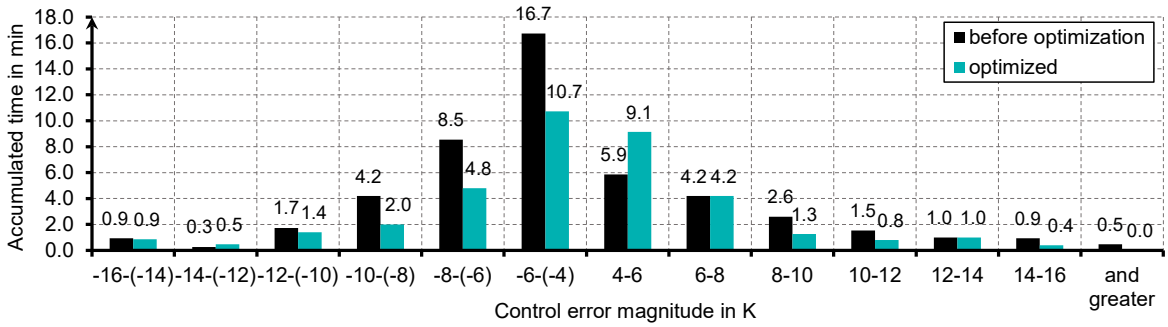

Figure 10. Accumulated time in which different control errors occur.

6. Conclusion

A control concept for a molten salt star-receiver was developed. The control parameters were optimized in a test cycle by minimizing a cost function. The control concept was tested in cloud passage scenarios based on real weather data. During these tests, the control system shows no sign of unstable behavior. During periods with moderate radiation gradients, the performance of the control system is sufficient. But with the given control system it is not possible to fully compensate the system dynamics which are dominated by the salt transport delay. That is why the temperature deviations during cloud passages, which cause sharp radiation steps, is high. Temperatures up to 580 °C are measured at the outlet of the receiver. Despite the limited performance due to the simple controller approach, the system is shown to be functional in the given test case and provides a starting point for further developments, like the integration of model predictive controllers.

In general, defining a cost function and minimizing the costs during a defined test cycle seems to be a useful approach to tune the controller parameters of solar thermal systems. Nevertheless, the main issue with the used control system is the inability to compensate the delay due to salt transport. The results of the optimization are also strongly dependent on the cost function and test cycle. Therefore the quality of the control system varies with the quality of the used cost function and the quality of the optimization scenario. To ensure that the current parameter set is optimal, more simulations with different scenarios and cost functions need to be carried out.

Data availability statement

The applied data are subject to third party IP and therefore not publically available.

Author contributions

J. Schulte: Conceptualization, Data curation, Formal Analysis, Funding acquisition, Investigation, Methodology, Software, Visualization, Writing – original draft; C. Schwager: Data curation, Funding acquisition, Methodology, Software, Project administration, Supervision, Writing – review & editing; C. Frantz: Data curation, Funding acquisition, Project administration; F. Schloms: Data curation; C. J. T. Boura: Project administration, Supervision, Writing – review & editing; U. Herrmann: Supervision, Writing – review & editing

Competing interests

The authors declare no competing interests.

Funding

This work is funded by the German Federal Ministry for Economic Affairs and Climate Action.

Acknowledgment

The authors gratefully acknowledge the support of the German Aerospace Center which provided the DNI-maps.

References

1. Michael Puppe, Stefano Giuliano, Cathy Frantz, Ralf Uhlig, Robert Flesch, Ralph Schumacher, et al. Techno-economic optimization of molten salt solar tower plants. AIP Conference Proceedings. 2018;2033:40033. doi: https://doi.org/10.1063/1.5067069.

2. Flesch R, Maldonado D, Schwarzbözl P. Dynamic Modelling of Molten Salt Central Receiver Systems. In: : ARGESIM Publisher Vienna; 2018. doi: https://doi.org/10.11128/arep.55.a55231.

3. Schwager C, Angele F, Schwarzbözl P, Boura CJT, Herrmann U. Model Predictive Assistance for Operational Decision Making in Molten Salt Receiver Systems. SolarPACES Conference 2021. 2021.

4. Bonk A, Rückle D, Kaesche S, Braun M, Bauer T. Impact of Solar Salt aging on corrosion of martensitic and austenitic steel for concentrating solar power plants. Solar Energy Materials and Solar Cells. 2019;203:110162. doi: https://doi.org/10.1016/j.solmat.2019.110162.

5. Schwager C, Flesch R, Schwarzbözl P, Herrmann U, Boura CJT. Advanced two phase flow model for transient molten salt receiver system simulation. Solar Energy. 2022;232:362–75. doi: https://doi.org/10.1016/j.solener.2021.12.065.

6. Nelder JA, Mead R. A Simplex Method for Function Minimization. The Computer Journal. 1965;7:308–13. doi: https://doi.org/10.1093/comjnl/7.4.308.

7. Nouri B, Blum N, Wilbert S, Zarzalejo LF. A Hybrid Solar Irradiance Nowcasting Approach: Combining All Sky Imager Systems and Persistence Irradiance Models for Increased Accuracy. Solar RRL. 2022;6:2100442. doi: https://doi.org/10.1002/solr.202100442.